Chapter 6
Characterization of nanofiber devices

6.1 The measurement problem

Previous chapters have introduced and described a variety of measurement techniques for RF nanoelectronic devices. Here, our objective is to work through an illustrative example that highlights strategies and challenges related to implementing a specific RF nanoelectronic device measurement. To that end, this chapter will describe the broadband, two-port characterization of an individual nanofiber device (Here, a "nanofiber" is broadly defined to be any individual nanotube or nanowire, or a bundle of nanotubes or nanofibers). Historically, the electromagnetic characterization of individual carbon nanotubes at gigahertz frequencies was one of the first measurement challenges encountered in the relatively short history of RF nanoelectronics [1]-[4]. Interest in making accurate RF measurements of nanotubes has been driven largely by the potential uses of carbon nanotubes as high-quality interconnects in very large scale integrated circuits and as nano-antennas in communications applications [5]. In addition, such measurements were needed to investigate what influence, if any, the quantum capacitance and kinetic inductance have on the AC transport properties of carbon nanotubes [6]. The techniques that were developed for electromagnetic characterization of carbon nanotubes have subsequently been applied to additional nano-material systems, including semiconducting nanowires and graphene nanoribbons [7]-[9].

The twofold goals of the measurement example presented in this chapter are: (1) to obtain de-embedded complex scattering parameters for the device and (2) to extract circuit model parameters that describe the electromagnetic properties of the device, including the nanofiber and its contacts. We will consider the specific case of a semiconducting GaN nanowire, though this measurement approach generally is applicable to any nanofiber. Note that this measurement approach is not the only approach to the problem, nor is it necessarily the best approach. Nonetheless, this example measurement concretely implements the strategies that have been presented in previous chapters.

First, we introduce the nanofiber device geometry and describe approaches to fabrication. Subsequently, we discuss calibrated, on-wafer measurements of the device, including the translation of the reference planes, which allows for complete de-embedding of the scattering parameters. We present a circuit model for the device and discuss the steps needed to extract relevant circuit model parameters from the de-embedded scattering parameters. Throughout this example, we present measured and de-embedded data for the specific case of a two-port device that incorporates an individual GaN nanowire.

6.2 Device geometry and fabrication

In order to characterize an individual nanofiber at microwave frequencies, the nanofiber must be integrated into a microwave host device. Here, we will consider a nanofiber that is integrated into a coplanar waveguide (CPW) structure as illustrated in Fig. 6.1. This simple, passive device represents a practical test platform for measuring electromagnetic material properties and for optimization of contact impedance. Advanced device applications will likely be more complex, but this design presents a suitable case study for

demonstration and discussion of the measurement approaches for extreme impedance devices in general and RF nanoelectronic devices in particular. In this device design, there is a small gap in the center conductor at the midpoint of the CPW. An individual nanofiber bridges this gap. The length of the gap is chosen to be between a few micrometers to tens of micrometers, depending on the length of the nanofiber under test. In this specific example, for an as-grown GaN nanowire with a length of about 10 μm, a 4 μm gap was chosen. To either side of the gap, the center conductor is tapered in order to constrain the area where the nanofiber can bridge the gap and to reduce the reflection of microwave signals that may result from an abrupt impedance mismatch. At either end of the host device, segments of CPW with a transmission line impedance of fifty ohms serve as landing sites for on-wafer, ground-signal-ground probes. Because of the high impedance of the nanofiber, a significant contribution to transmission through the device will be made by parasitic coupling across the gap in the center conductor. Thus, following the strategy laid out in Chapters 4 and 5, an empty, nanofiber-free device that is otherwise identical to the device show in Fig. 6.1 is fabricated on the same wafer.

Figure 6.1. **Geometry of a nanowire device.** A CPW host device for broadband characterization of nanowire devices is illustrated (Top View). The CPW host structure is illustrated in gray, the nanowire is illustrated in black. The on-wafer, multiline thru-reflect-line (TRL) calibration establishes reference planes at positions R_0. Subsequently, the reference planes are rolled to position R_1.

In practice, there are several approaches to fabricating a microwave nanofiber device. One approach is to fabricate the CPW host by use of standard photolithography techniques and then affix an individual nanofiber in the device by use of a focused ion beam (FIB) [10]. A nano-manipulator is used to transfer an individual nanofiber into the gap in the CPW host. Subsequently, the ends of the nanofiber may be fixed by metal bonds formed by use of FIB-induced deposition. These metal bonds also serve as electrical contact points between the fiber and the host structure, thus contributing to the contact impedance. The FIB-based approach enables precise control of fiber positioning and contact formation. Furthermore, this approach allows for real-time inspection of the device as FIB capabilities are typically integrated into dual-beam systems with scanning electron microscopes. However, this approach is time-consuming and devices are produced one-by-one. Furthermore, the contact impedance is difficult to control and reproduce. Lastly, the ion beam may damage the nanofiber.

A higher-throughput alternative to the FIB-based approach is to align the individual fibers with dielectrophoresis. During this process, a sinusoidal AC voltage signal is applied across the CPW gap. For the GaN nanowires discussed in detail in this chapter, this signal has a frequency between 50 kHz and 100 kHz and a peak-to-peak amplitude between 10 V and 20 V [11]. As the signal is being applied, a drop of nanofibers suspended in solution is dispensed over each device site and allowed to evaporate. Due to the presence of the AC field, some of the individual nanofibers will be induced to align themselves across the gaps in the devices. The aligned nanofibers can be subsequently secured by deposition of a photo-lithographically-defined layer on top of the contact area. A nanofiber device produced by use of this approach is shown in Fig. 6.2. Note that dielectrophoresis requires electrical contacts to the center conductor of each CPW device on the wafer. Though this approach yields

multiple devices, the yield is significantly less than one hundred percent and some fraction of the devices may have more than one nanofiber per gap.

Figure 6.2. **Scanning electron microscope image of a GaN nanowire device.** The image shows an individual GaN nanowire bridging a 4 μm gap in a two-port, CPW host device.

Though this device geometry is simple and the fabrication steps described above appear straightforward, the fabrication of this two-port nanoelectronic device presents several significant challenges. The first barrier is the need for high-quality nano-materials. In the case of GaN nanowires, the wires were grown via plasma-assisted molecular beam epitaxy. The as-grown nanowires were essentially defect-free and could be removed from the growth substrate by ultrasonic agitation in isopropanol. This yielded a nanowire solution amenable to dielectrophoresis, though the use of extremely small (~μL) drops of solution placed only upon the gap in the CPW was required in order to prevent unwanted placement of stray wires in locations other than the gap in the CPW. Once the wires were placed, they were secured with appropriate metal deposition.

The next fabrication challenge is substantial: the electromagnetic properties of the resulting contact regions between the GaN nanowire and the metal host structure must be controlled. In general, the control and optimization of electrical contacts to nano-materials is one of the most difficult steps in the fabrication of RF nanoelectronic devices. In the specific case of GaN nanowires, the fabrication of ohmic contacts to the wire requires several key steps, including appropriate choice of contact materials that may depend on the wire conductivity and carrier type (e.g. Ti and Al for n-type GaN) as well as a reactive ion etch treatment of the wires before metal deposition. Generally, contact optimization in the device development phase generally follows an iterative process, cycling through repeated fabrication and characterization steps. For more complex devices, such as nanowire transistors, which incorporate multiple material components and three or more contacts to the nanowire, fabrication naturally becomes increasingly challenging and complex [3],[7],[11].

Before describing the measurements themselves, it is useful to point out how strategic device design and fabrication approach must be developed in conjunction with the identification of measurement approaches. As a simple example, additional "empty" devices, as well as other calibration devices that will be discussed in more detail below, must be fabricated along with the device under test. In a case where multiple measurement approaches are under consideration, it is conceivable that multiple sets of calibration standards may need to be included in the design. A subtler issue is that the design choice to include tapered sections of CPW will have implications for modeling the circuit and extracting model parameters, as will also be discussed below.

6.3 Calibrated on-wafer measurements

The next step is calibrated, on-wafer measurement of the device and de-embedding of the device's two-port scattering parameters from the test platform. As outlined in earlier chapters, there are a number of well-known on-wafer calibration procedures to choose from, including short-open-load-thru (SOLT), line-reflect-reflect-match (LRRM), and multiline thru-reflect line (TRL). Here, we select multiline TRL [12] because it enables rolling of the reference planes of the measurement from their original position (labeled R_0 in Fig. 6.1) to a new location closer to the nanowire and its contact points (labeled R_1 in Fig. 6.1). By translating the reference planes in this way, the influence of the CPW segments at either end of the device can effectively be taken out of the device measurement.

Figure 6.3. **Layout of nanowire devices and calibration devices.** Four nanowire devices under test, four empty (nanowire-free) devices, and six on-wafer calibration structures are illustrated. The six on-wafer calibration structures, including a thru, a short, and four transmission lines, are used to perform a thru-reflect-line (TRL) calibration. The empty devices are used to extract the stray capacitance, as discussed in the text.

Each on-wafer calibration method requires the fabrication of a set of on-wafer calibration devices. Ideally, these calibration devices will be fabricated on the same substrate as the devices under test (DUTs). For multiline TRL, the following CPW calibration devices are required: a thru (chosen here to be 0.500 mm long), a short circuit, and multiple transmission lines of differing lengths (chosen here to be 1.80 mm, 2.60 mm, 3.83 mm, and 6.10 mm). A typical wafer layout is illustrated in Fig. 6.3, including nanowire devices, empty reference devices, and a set of calibration devices. Note that we have implemented a ground-signal-ground configuration for each CPW calibration standard as well as the CPW nanowire device. Other configurations, such as ground-signal, are possible, but with corresponding trade-offs in device footprint, device performance, and measurement uncertainty.

To perform the calibrated measurements, each of the on-wafer standards is measured by use of a two-port, on-wafer probe station. Subsequently, every DUT, including at least one nanowire device and one empty device, is measured with the same probes. The measured scattering parameters of the calibrations standards are processed via the calibration algorithm in order to determine the error boxes. The error boxes are then used to de-embed the scattering parameters of the nanowire device and empty device. In a TRL calibration, the complex scattering coefficient is also found by the calibration algorithm. In practice, it is useful to re-measure each on-wafer standard again at the conclusion of the experiment. This second set of calibration standard measurements provides an additional data set and quantitative estimate of statistical uncertainty in the calibration procedure.

Figure 6.4. **Raw s-parameter measurement of GaN nanowire device.** The magnitudes of the raw, uncalibrated scattering parameters, S^M_{11} and S^M_{21}, are shown as a function of frequency, as measured with a vector network analyzer. Measurements of a nanowire

device, $\mathbf{S}^{\mathbf{M\text{-}total}}$, (solid black curve) and an empty reference device, $\mathbf{S}^{\mathbf{M\text{-}empty}}$, (dashed gray curve) are shown.

The magnitudes of the as-measured, uncalibrated scattering parameters, $S^{M}{}_{11}$ and $S^{M}{}_{21}$, are shown in Fig. 6.4, for both the nanowire device and the empty device. The full measured, two-port scattering parameter matrices for the nanowire device and for the empty device are represented by $\boldsymbol{S}^{\boldsymbol{M\text{-}total}}$ and $\boldsymbol{S}^{\boldsymbol{M\text{-}empty}}$, respectively. Keep in mind that the elements of the scattering parameter and admittance matrices discussed in this case study are complex valued. For simplicity, we will focus on the magnitudes of these elements throughout the discussion. Over the frequency range shown in Fig. 6.4, differences in $S^{M}{}_{21}$ for the nanowire and empty devices are observable, though the difference decreases as the measurement frequency increases. Meanwhile little difference is discernable for $S^{M}{}_{11}$.

The TRL procedure yields the corresponding calibrated, two-port scattering parameters, $\boldsymbol{S}^{\boldsymbol{C\text{-}total}}$ and $\boldsymbol{S}^{\boldsymbol{C\text{-}empty}}$. By default, the reference planes of the calibrated measurement are displaced from each end of the host device by 0.250 mm (half the length of the thru standard). The location of these reference planes are labeled as R_0 in Fig. 6.1. Because the TRL algorithm extracts the complex propagation constant in addition to the error boxes, it is possible to roll the reference planes to a new position at the boundary between the straight and tapered sections of the host CPW, labeled as R_1 in Fig. 6.1.

A few algebraic manipulations are required to transform a calibrated scattering parameter matrix $\boldsymbol{S}^{\boldsymbol{C}}$ with reference planes at R_0 to a calibrated scattering parameter matrix $\boldsymbol{S}^{\boldsymbol{C'}}$ with reference planes at R_1. The first step is to transform $\boldsymbol{S}^{\boldsymbol{C}}$ into a transmission matrix $\boldsymbol{T}^{\boldsymbol{C}}$. The propagation constant γ is known from the TRL algorithm. The distance between R_0 and R_1 is L. A transmission matrix $\boldsymbol{T}^{\boldsymbol{L}}$ for a line with propagation constant γ and length L can be constructed as follows:

$$\boldsymbol{T}^{\boldsymbol{L}} = \begin{bmatrix} e^{-\gamma L} & 0 \\ 0 & e^{\gamma L} \end{bmatrix} . \tag{6.1}$$

A new transmission matrix with reference planes at R1 can be formed from

$$\boldsymbol{T}^{\boldsymbol{C'}} = (\boldsymbol{T}^{\boldsymbol{L}})^{-1}\, \boldsymbol{T}^{\boldsymbol{C}}\, \boldsymbol{T}^{\boldsymbol{L}} \ . \tag{6.2}$$

As a final step, the transmission matrix $\boldsymbol{T}^{\boldsymbol{C'}}$ is transformed back to a scattering parameter matrix $\boldsymbol{S}^{\boldsymbol{C'}}$. Note that the above analysis assumes that all transmission matrices share the same reference impedance. If the transmission matrices do not share the same reference impedance, then additional algebraic steps will be required to transform the impedances.

Figure 6.5. **De-embedded s-parameter measurement of GaN nanowire device.** The magnitudes of the de-embedded, calibrated scattering parameters, S_{11} and S_{21}, with the reference planes translated to position R_1, are shown as a function of frequency. Measurements of a nanowire device, $\boldsymbol{S}^{\boldsymbol{total}}$, (solid black curve) and an empty reference device, $\boldsymbol{S}^{\boldsymbol{empty}}$, (dashed gray curve) are shown.

The magnitudes of the calibrated, transformed scattering parameters for the nanowire and empty device with the reference planes rolled to the new position R_1, $\boldsymbol{S}^{total}$ and $\boldsymbol{S}^{empty}$, are shown in Fig. 6.5. As with the uncalibrated scattering parameters, clear differences are discernable in S_{21} but not in S_{11}. Note that the frequency-dependent ripples in the measurements shown in in Fig. 6.4 have been eliminated. The de-embedded scattering parameters shown in Fig. 6.5 are now smooth curves as a function of frequency.

Ultimately, the objective is to de-embed the properties of the nanowire and its contacts from the properties of the host structure. In particular, we seek to determine $\boldsymbol{S}^{nw}$, the complex scattering parameter matrix of the nanowire and its contacts. The location of reference plane R_1 implies that $\boldsymbol{S}^{nw}$ also includes the influence of the tapered CPW sections. The de-embedding is more easily accomplished if the scattering parameter matrices are transformed to an impedance matrix representation. $\boldsymbol{S}^{total}$ and $\boldsymbol{S}^{empty}$ are transformed to impedance matrices $\boldsymbol{Y}^{total}$ and $\boldsymbol{Y}^{empty}$, which are related to $\boldsymbol{Y}^{nw}$, the impedance matrix of the nanowire and its contacts, in the following way:

$$\boldsymbol{Y}^{total} = \boldsymbol{Y}^{nw} + \boldsymbol{Y}^{empty} . \qquad (6.3)$$

$\boldsymbol{Y}^{nw}$ is readily determined by use of equation 6.3. Fig. 6.6 shows the magnitudes of elements of the impedance matrices $\boldsymbol{Y}^{total}$, $\boldsymbol{Y}^{empty}$, and $\boldsymbol{Y}^{nw}$. Comparing $\boldsymbol{Y}^{total}$ and $\boldsymbol{Y}^{empty}$, clear differences are discernable in both Y_{11} and Y_{21}. Note that the linear dependence of $\boldsymbol{Y}^{empty}{}_{21}$ on frequency is consistent with purely capacitive coupling across the empty gap. As a final step, the complex matrix $\boldsymbol{Y}^{nw}$ may be converted to $\boldsymbol{S}^{nw}$, as shown in Fig. 6.6(d).

Figure 6.6. **Calibrated measurement of GaN nanowire scattering parameters.** (a) and (b) Magnitudes of the admittance matrix elements Y_{11} and Y_{21} of the matrices $\boldsymbol{Y}^{total}$ and $\boldsymbol{Y}^{empty}$. (c) Magnitudes of the admittance matrix elements Y_{11} and Y_{21} of the matrix $\boldsymbol{Y}^{nw}$. (d) Magnitudes of the scattering matrix elements S_{11} and S_{21} of the matrix $\boldsymbol{S}^{nw}$.

6.4 Uncertainty analysis

Uncertainty analysis is a vital step in establishing reliable metrology tools for emerging application areas. Unfortunately, this step has often been overlooked during RF and microwave measurements of nanoelectronic devices. Consider the measurements of the magnitude of the admittance parameters of the GaN nanowire devices, $Y^{nw}{}_{11}$ and $Y^{nw}{}_{21}$, shown in Fig. 6.6. It is clear that the magnitude of $Y^{nw}{}_{21}$ is quite small with a maximum value of about one mS. A reliable uncertainty analysis is particularly important in the measurement of such small quantities where the value of the uncertainty may represent a significant fraction of the value of the measurand. Below, we will estimate the uncertainty budget for the measurement of the GaN nanowire devices.

Before discussing the specific case of the two-port nanowire device measurement, it is useful to review several core concepts of uncertainty analysis. Suppose there are N different components of uncertainty in a measurement process. Let u_i be the standard uncertainty for component i (i = 1, 2, … N) and let u_i be equal to the positive square root of the

estimated variance. If the components of uncertainty are uncorrelated, one simple way to estimate the total standard uncertainty is

$$u_{total} = \sqrt{{u_1}^2 + {u_2}^2 \ldots + {u_N}^2} \ . \tag{6.4}$$

In describing contributions of different components of uncertainty, it is useful to distinguish between methods used to estimate the uncertainty values [13]. Uncertainties determined from the statistical analysis of multiple, repeated measurements are referred to as "Type A" uncertainties. For example, Type A uncertainties may be calculated from repeated measurements of the same system as well as from measurements of multiple, nominally identical, systems. Uncertainties determined from non-statistical methods are referred to as "Type B" uncertainties. Examples of Type B uncertainties include uncertainties calculated from physical models or uncertainties taken from manufacturer specifications.

Returning to the example of the two-port nanowire devices, the measurement process rests on the calibrated, on-wafer measurement of two scattering parameter matrices, $\boldsymbol{S^{total}}$ and $\boldsymbol{S^{empty}}$. Let $\Delta S^{total}{}_{ij}$ and $\Delta S^{empty}{}_{ij}$ be the uncertainties in the matrix element ij of these scattering parameter matrices. As the scattering parameters are transformed to an admittance representation, the uncertainties will propagate in the following way:

$$\Delta Y^{total}{}_{ij} = \sqrt{\sum_{k,l} \left(\frac{\partial Y^{total}{}_{ij}}{\partial S^{total}{}_{kl}} \Delta S^{total}{}_{kl} \right)^2} \tag{6.5}$$

And

$$\Delta Y^{empty}{}_{ij} = \sqrt{\frac{(\Delta Y^{A-empty}{}_{ij})^2}{N_{empty}} + \sum_{k,l} \left(\frac{\partial Y^{empty}{}_{ij}}{\partial S^{empty}{}_{kl}} \Delta S^{empty}{}_{kl} \right)^2} \ . \tag{6.6}$$

The partial derivatives of the form $\delta Y/\delta S$ are determined from the equations that prescribe the transformation from scattering parameters to admittance parameters [14]. Note the inclusion of the Type A uncertainty term $\Delta Y^{\text{A-empty}}{}_{\text{ij}}$, in equation (6.6). This term is included because imperfections in the fabrication process and substrate inhomogeneity may lead to variations of geometric and electromagnetic properties from device to device. The value of $\Delta Y^{A\text{-}empty}{}_{ij}$ is estimated from statistical analysis of N_{empty} repeated measurements of empty devices. Once $\Delta Y^{total}{}_{ij}$ and $\Delta Y^{empty}{}_{ij}$ are known, the total uncertainty in the magnitude of the elements of $\boldsymbol{Y^{nw}}$ is given by

$$\Delta Y^{nw}{}_{ij} = \sqrt{(\Delta Y^{empty}{}_{ij})^2 + (\Delta Y^{total}{}_{ij})^2 + (\Delta Y^{B}{}_{ij})^2 + \frac{(\Delta Y^{A-nw}{}_{ij})^2}{N_{repeat}}} \tag{6.7}$$

Further variations from measurement to measurement may result from lack of repeatability in the position of the ground-signal-ground probes on the device. To account for this component of the uncertainty, the measurement of a given nanowire device is repeated N_{repeat} times and the Type A uncertainty term $\Delta Y^{A\text{-}nw}{}_{ij}$ is determined from statistical analysis of the resulting measurements. A single Type B uncertainty term, $\Delta Y^{B\text{-}nw}{}_{ij}$, is included to account for systematic sources of uncertainty in the measurement process, including the validity (or lack of validity) of equation 6.3.

Table 6.1. **Typical uncertainty budget for the magnitude of the admittance matrix elements Y^{nw}_{ij} of a two-port nanowire device.**

Uncertainty Component	***k=2 Value at 10 GHz***	***k=2 Value at 35 GHz***
ΔS^{total}	0.005	0.005
ΔS^{empty}	0.005	0.005
$\Delta Y^{A\text{-}empty}$	0.005 mS	0.025 mS
ΔY^{total}	0.050 mS	0.050 mS
ΔY^{empty}	0.050 mS	0.055 mS
$\Delta Y^{A\text{-}nw}$	0.015 mS	0.030 mS
ΔY^{B}	0.050 mS	0.050 mS
ΔY^{nw}	0.085 mS	0.090 mS

A typical uncertainty budget for the magnitude of the admittance matrix elements Y^{nw}_{ij} of a two-port nanowire device, based on the estimation process described above, is shown in Table 6.1. The values of ΔS^{total}_{ij}, ΔS^{empty}_{ij}, and $\Delta Y^{B\text{-}nw}_{ij}$ are estimated from the literature [15], [16]. Note that the Type A uncertainty values, $\Delta Y^{A\text{-}empty}_{ij}$ and $\Delta Y^{A\text{-}nw}_{ij}$, vary the strongest between the two frequencies shown in the table. The coverage factor k is two for the uncertainty components shown in the table, i.e. they correspond to twice the standard uncertainty. When the complete uncertainty calculation is carried out via equation 6.4, the estimated uncertainty ΔY^{nw}_{ij} is about 0.085 mS at 10 GHz and 0.090 mS at 30 GHz. Comparison to Fig. 6.6 reveals that these uncertainty estimates represents a significant fraction of the value of Y^{nw}_{11}, namely about 75% of Y^{nw}_{11} at 10 GHz and about 15% of Y^{nw}_{11} at 30 GHz. Further comparison to Fig. 6.6 reveals that these uncertainty estimates exceed the value of Y^{nw}_{21} throughout the measured frequency range. The significant uncertainties of this measurement technique imply that any circuit or material parameters extracted from these measurements should be treated as estimates at best. The largest contribution to the total uncertainty comes from the uncertainty in the calibrated, on-wafer measurement of scattering parameter matrices, as propagated via equations 6.5 and 6.6. Estimation and minimization of uncertainties in calibrated on-wafer measurements are ongoing challenges, but do provide a way forward for improving both on-wafer measurements in general as well as RF nanoelectronic device measurements in particular.

On-wafer implementation of the extreme impedance techniques introduced in Chapter 3 may also provide an avenue to finding a measurement approach with lower uncertainties.

6.5 Extraction of parameters from circuit models

In some cases, the calibrated measurement of the de-embedded scattering parameters of the device, $\mathbf{S}_{nw}$, may be sufficient. However, in a research and development environment, additional information about the nanoelectronic device may be sought. In the case of the simple, prototype GaN nanowire device discussed in this chapter, a number of questions may be asked. What are the intrinsic electromagnetic material properties of the nanowire? Are the contacts Schottky-like or ohmic? Are there strong differences between the contacts at either end of the nanowire? Are there strong variations in the scattering parameters from device to device? In order to address such questions, we will develop a circuit model for the device and extract corresponding circuit parameters.

As discussed in Chapter 5, circuit models of RF nanoeletronic devices often combine both distributed and lumped elements. Nanofibers with different physical properties may be better represented by alternative choices within a circuit model. For example, a metallic nanowire may be represented by a simple, lumped-element resistor, provided that its length is much shorter than the wavelength in the experiment. For some nanomaterials, such as graphene and carbon nanotubes, being measured at high enough frequencies, quantum phenomena such as kinetic inductance and quantum capacitance may make a significant contribution. In such cases, appropriate circuit elements must be added to the model.

Figure 6.7. **Circuit models for a nanowire device and an empty device.** (a) Circuit model for a nanowire device, including contact resistance (R_c) and electrostatic contact capacitance (C_c), as well as a π-network representing the nanowire. (b) Circuit model for the empty, nanowire-free device. Both models include the tapered section of the coplanar waveguide host as well as the parasitic capacitance C_{gap}.

Fig. 6.7 shows possible circuit models of the two-port GaN nanowire device, with and without the nanowire and its contacts. In this model, the contact resistance R_c, electrostatic contact capacitance C_c, and parasitic capacitance C_{gap} are represented by lumped elements while the nanowire itself and the tapered segments to either side of the wire are modeled as distributed elements. The contact capacitance C_c may make a significant contribution in certain nanofiber devices, such as carbon nanotubes. Here, in the case of annealed GaN nanowires with Ohmic contacts, $(\omega\ C_c)^{-1} \gg R_c$. Thus, C_c will be ignored for the remainder of the discussion. The tapered segments are modeled as a finite series of CPW transmission lines with successively narrower center conductor widths. The models of the tapered segments are parameterized by an effective length, l_{taper}. Finally, the GaN nanowire is represented by a π-network. The admittance of each element of the π-network is proportional to the characteristic complex admittance Y of an equivalent transmission line

$$Y = \sqrt{\frac{G_{nw}+j\omega C_{nw}}{R_{nw}+j\omega L_{nw}}} \tag{6.8}$$

where R_{nw}, L_{nw}, G_{nw}, and C_{nw} are the per unit length series resistance, series inductance, shunt conductance, and shunt capacitance, respectively. We require that if one of the two ports of the π-network is loaded with a characteristic impedance $Z = 1/Y$, the total impedance at the unloaded port will be Z. This requirement leads to a value of the constant $\alpha = 2 / \sqrt{5}$. In the specific example of the GaN nanowire device, G_{nw} and L_{nw} are negligible, i.e. $R_{nw} \gg \omega L_{nw}$ and $\omega C_{nw} \gg G_{nw}$. The complex scattering parameters of the model network can be calculated with a commercial software package. Subsequently, the unknown parameters can be adjusted to fit the model response to the calibrated, measured scattering parameter data.

Table 6.2. **Typical circuit parameters for a two-port GaN nanowire device.**

Parameter	***Value***
C_{gap}	690 aF
l_{taper}	130 µm
R_{nw}	58 kΩ / µm
C_{nw}	6500 aF / µm
R_c	3.6 kΩ

The model has five unknown parameters: R_c, C_{gap}, l_{taper}, R_{nw}, and C_{nw}. Two of these parameters, C_{gap} and l_{taper}, may be determined by fitting the modeled scattering parameters of the empty device to the measured scattering parameters. This initial fitting procedure requires that the model of the nanowire device be modified to represent an empty device by removing the π-network that represents the nanowire as well as the lumped elements representing the contacts (R_c and C_c). Once C_{gap} and l_{taper} are known, the remaining unknown parameters, R_c and the ratio R_{nw} / C_{nw}, may be determined by fitting the modeled scattering parameters for the full nanowire device to the measured scattering parameters. R_{nw} may then be determined by enforcing the condition that the DC resistance equal the sum of the wire resistance and twice the contact resistance. As we have seen in other cases, unique determination of contact and nanowire properties requires additional measurements, in this case in the form of a DC resistance measurement. Alternatively, the measured nanowire device data may be fit with R_C fixed to a reasonable value [17]-[19], leaving the ratio R_{nw} / C_{nw} as the only remaining fitting parameter. Typical values for R_c,

C_{gap}, l_{taper}, R_{nw}, and C_{nw} for a two-port GaN nanowire device [9] are summarized in Table 6.2.

References

[1] Z. Yu and P. J. Burke, "Microwave transport in metallic single-walled carbon nanotubes," *Nano Letters*, **5** (2005) pp. 1403-1406.

[2] M. Zhang, X. Huo, P. C. H. Chan, Q. Liang, and Z. K. Tang, "Radio-frequency characterization for the single-walled carbon nanotubes," *Applied Physics Letters*, **88** (2006) art. no. 163109.

[3] J. M. Bethoux, H. Happy, G. Dambrine, V. Derycke, M. Goffman, and J. P. Burgoin, "An 8-GHz f_t carbon nanotube field-effect transistor for gigahertz range applications," *IEEE Electron Device Letters*, **27** (2006) pp. 681-683.

[4] J. J. Plombon, K. P. O'Brien, F. Gstrein, V. M. Dubin, and Y. Jiao, "High-frequency electrical properties of individual and bundled carbon nanotubes," *Applied Physics Letters,* **90** (2007) art. no. 063106.

[5] P. Russer, "Nanoelectronics-based integrated antennas," *IEEE Microwave Magazine* **11** (2010) pp. 58-71.

[6] C. Rutherglen and P. J. Burke, "Nanoelectromagnetics: Circuit and Electromagnetic Properties of Carbon Nanotubes," *Small*, **5** (2009) p. 884-906.

[7] S. Vandenbrouck, K. Madjour, D. Théron, Y. Dong, Y. Li, C. M. Lieber, and C. Gaquiere, "12 GHz F_{MAX} GaN/AlN/AlGaN nanowire MISFET," *IEEE Electron Device Letters*, **30** (2009) pp. 322-324.

[8] S. Salahuddin, M. Lundstrom, and S. Datta, "Transport effects on signal propagation in quantum wires," *IEEE Transactions on Electron Devices*, **52** (2005) pp. 1734-1742.

[9] T. Mitch Wallis, Dazhen Gu, Atif Imtiaz, Christopher S. Smith, Chin-Jen Chiang, Pavel Kabos, Paul T. Blanchard, Norman A. Sanford, and Kris A. Bertness, "Electrical Characterization of Photoconductive GaN Nanowires from 50 MHz to 33 GHz," *IEEE Transactions on Nanotechnology* **10** (2011) 832-834.

[10] P. Rice, T. M. Wallis, S. E. Russek, and P. Kabos, "Broadband electrical characterization of multiwalled carbon nanotubes and contacts," *Nano Letters*, **7** (2007) pp. 1086-1090.

[11] P. T. Blanchard, K. A. Bertness, T. E. Harvey, L. M. Mansfield, A. W. Sanders, and N. A. Sanford, "MESFETS made from individual GaN nanowires," *IEEE Transactions on Nanotechnology*, **7** (2008) pp. 760-765.

[12] R. B. Marks, "A multiline method of network analyzer calibration," *IEEE Transactions on Microwave Theory and Techniques*, **39** (1991) pp. 1205-1215.

[13] ISO, *Guide to the Expression of Uncertainty in Measurement*. Geneva, Switzerland: International Organization for Standardization, 1993.

[14] D. M. Pozar, *Microwave Engineering*. Reading, MA: Addison-Wesley, 1993, p. 235.

[15] D. F. Williams, C. M. Wang, and U. Arz, "An Optimal Multiline TRL Calibration Algorithm" *2003 IEEE MTT-S International Microwave Symposium Digest*, **1-3** (2003) pp. 1819-1822.

[16] Kichul Kim, T. Mitch Wallis, Paul Rice, Chin-Jen Chiang, Atif Imtiaz, Pavel Kabos and Dejan S. Filipovic, "A Framework for Broadband Characterization of Individual Nanowires," *IEEE Microwave and Wireless Component Letters*, **20** (2010) pp. 178-180.

[17] L. M. Mansfield, K. A. Bertness, P. T. Blanchard, T. E. Harvey, A. W. Sanders, and N. A. Sanford, "GaN nanowire carrier concentration calculated from light and dark resistance measurements," *Journal of Electronic Materials* **38** (2009) pp. 495-504.

[18] N. A. Sanford, P. T. Blanchard, K. A. Bertness, L. Mansfield, J. B. Schlager, A. W. Sanders, A. Roshko, B. B. Burton, and S. M. George, "Steady-state and transient

photoconductivity in c-axis GaN nanowires grown by nitrogen-plasma-assisted molecular beam epitaxy," *Journal of Applied Physics* **107** (2010) art. no. 034318.

[19] N. A. Sanford, L. H. Robins, P. T. Blanchard, K. Soria, B. Klein, B. S. Eller, K. A. Bertness, J. B. Schlager, and A. W. Sanders, "Studies of photoconductivity and field effect transistor behavior in examining drift mobility, surface depletion, and transient effects in Si-doped GaN nanowires in vacuum and air," *Journal of Applied Physics* **113** (2013) art. no. 174306.

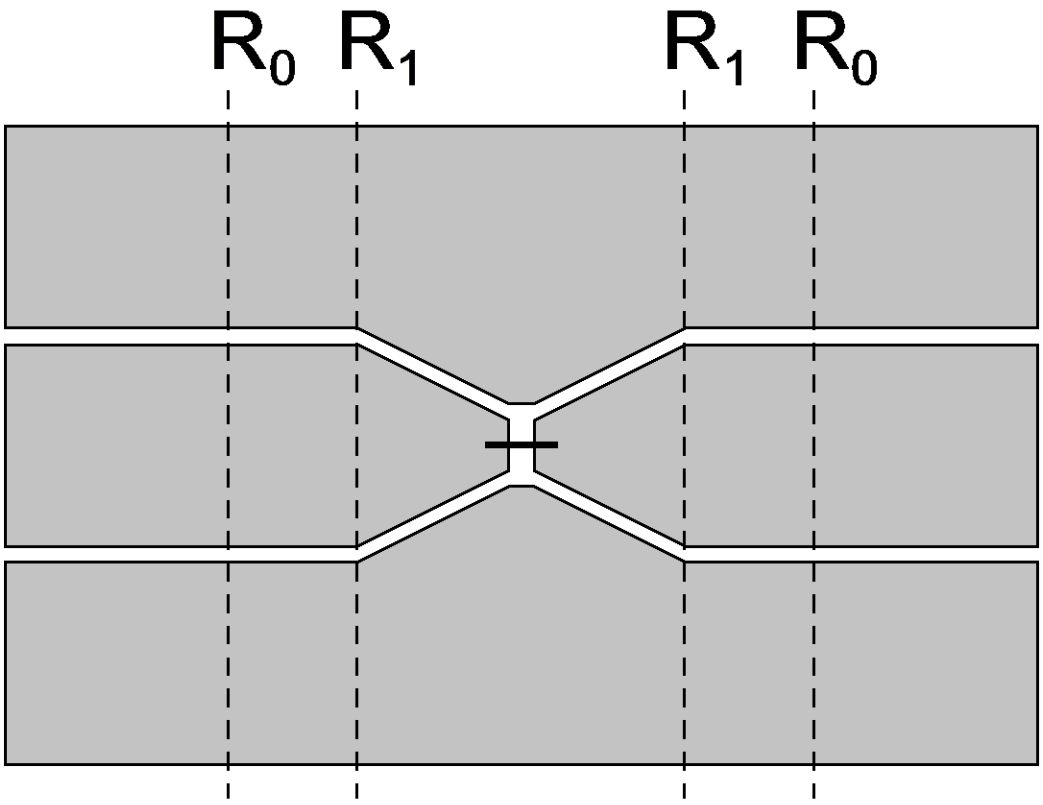

FIGURE 6-1.

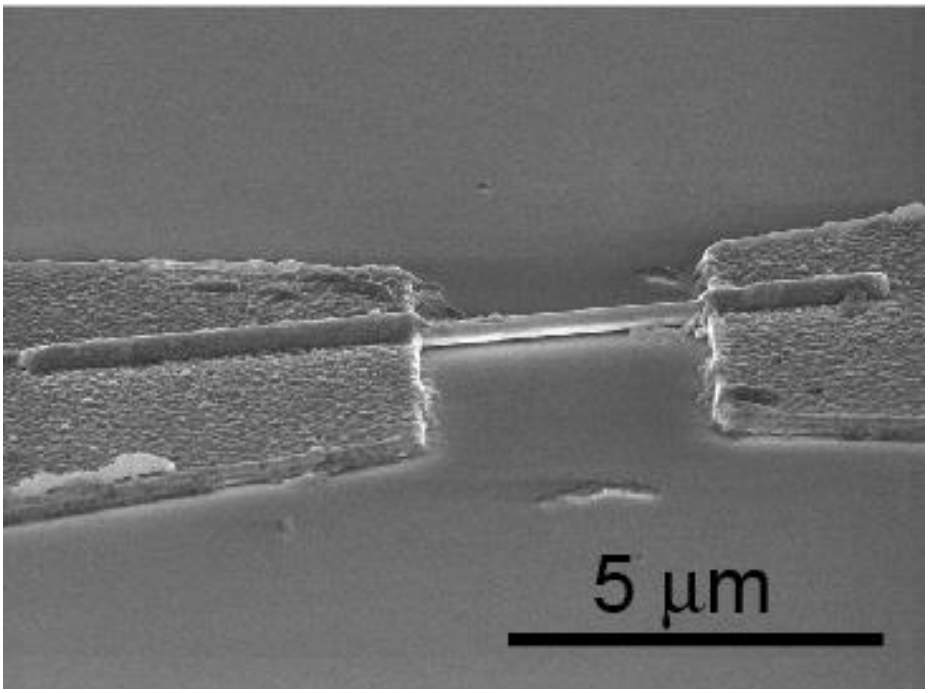

FIGURE 6-2.

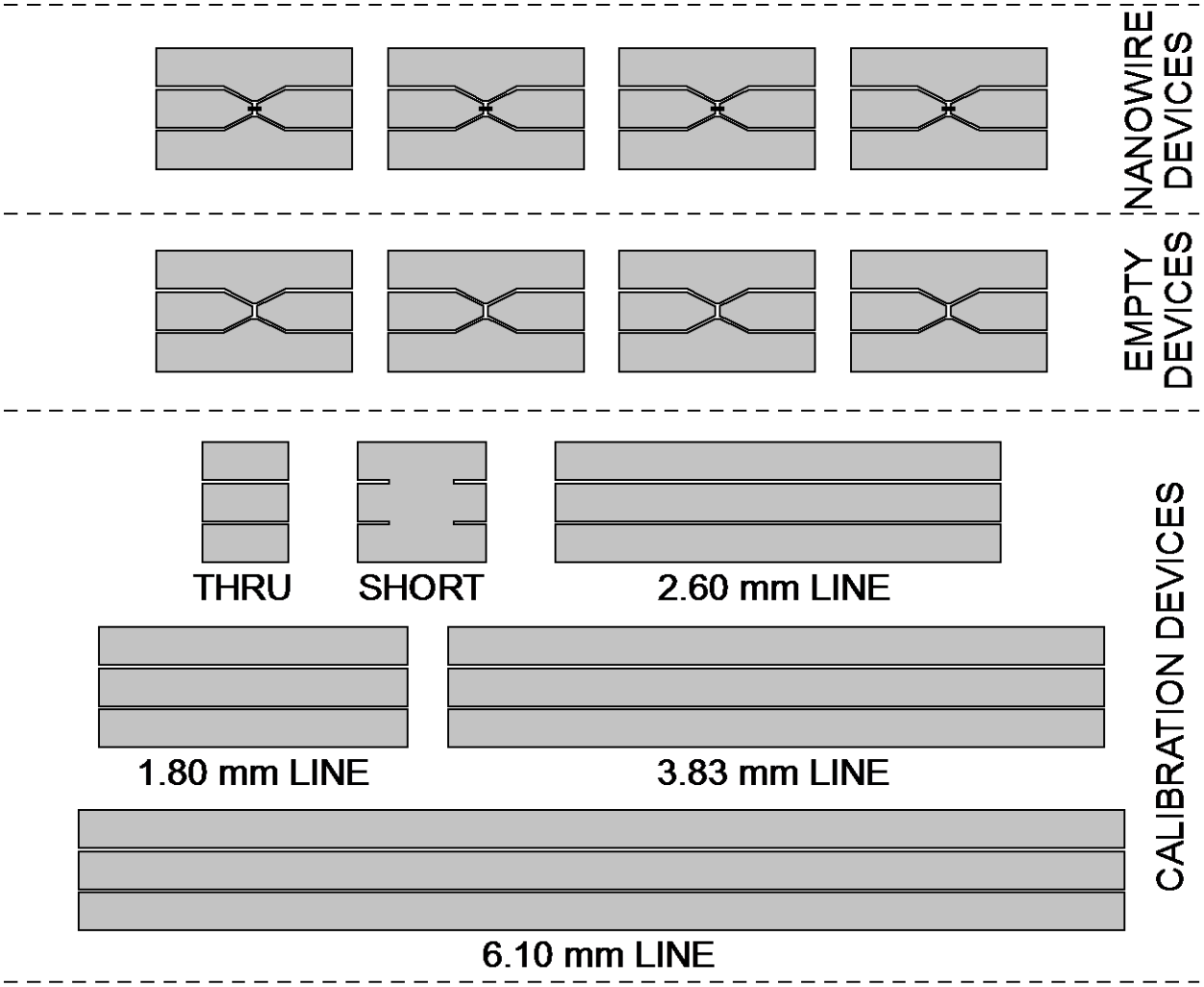
NANOWIRE DEVICES
EMPTY DEVICES
CALIBRATION DEVICES
THRU
SHORT
2.60 mm LINE
1.80 mm LINE
3.83 mm LINE
6.10 mm LINE

FIGURE 6-3.

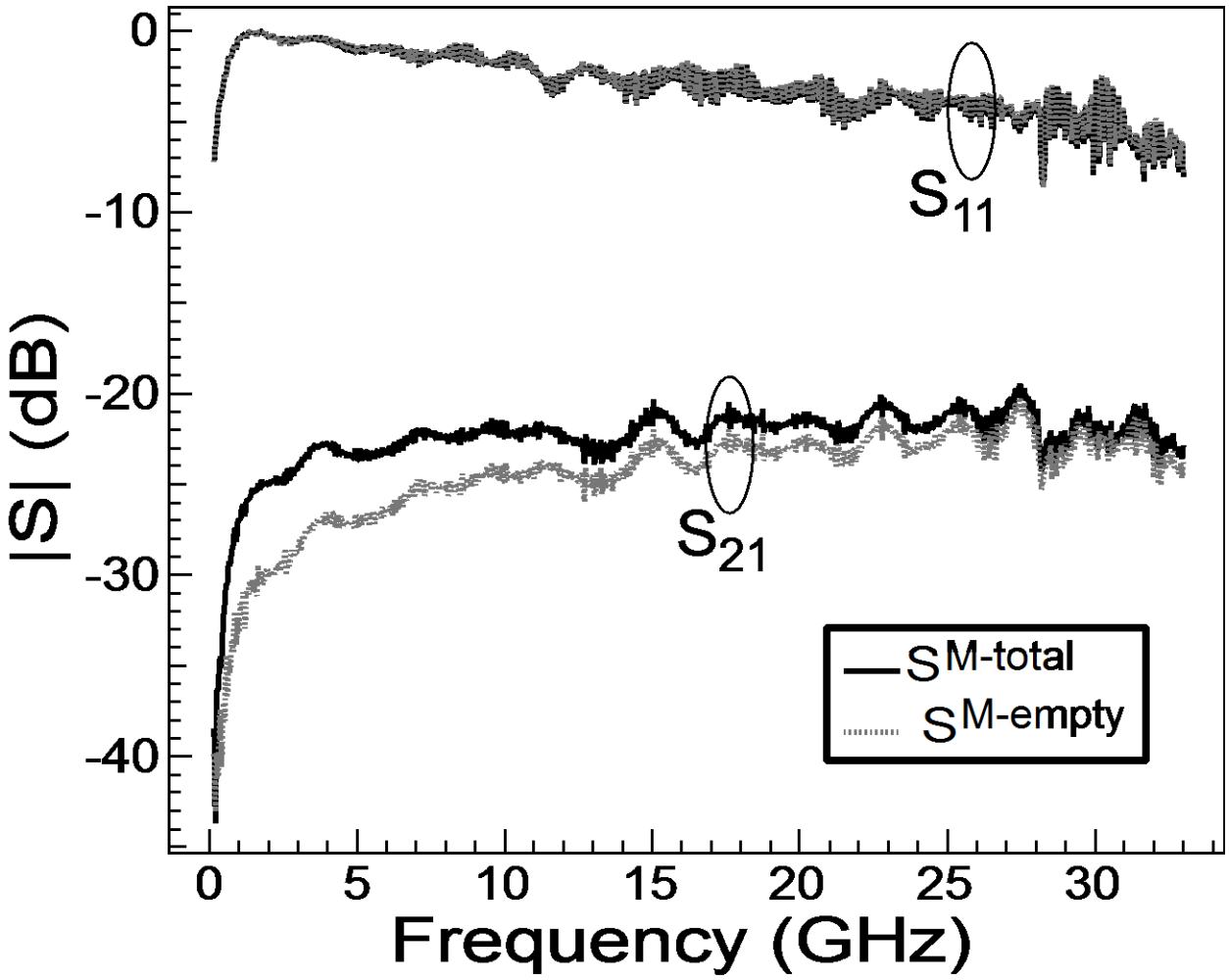
0
-10
-20
-30
-40
|S| (dB)
S11
S21
SM-total
SM-empty
0
5
10
15
20
25
30
Frequency (GHz)

FIGURE 6-4.

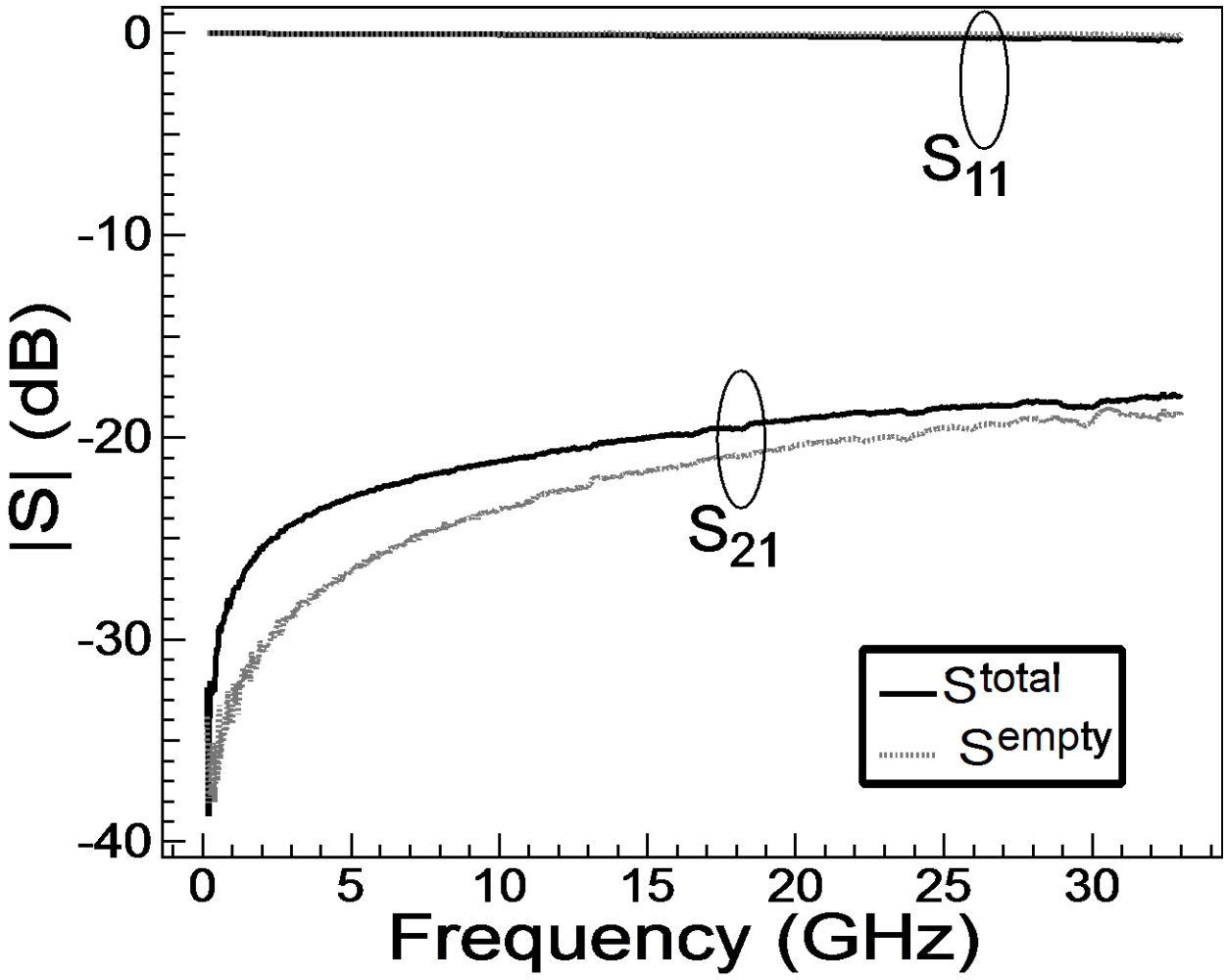
0
-10
-20
-30
-40
|S| (dB)
0
5
10
15
20
25
30
Frequency (GHz)
S11
S21
Stotal
Sempty

FIGURE 6-5.

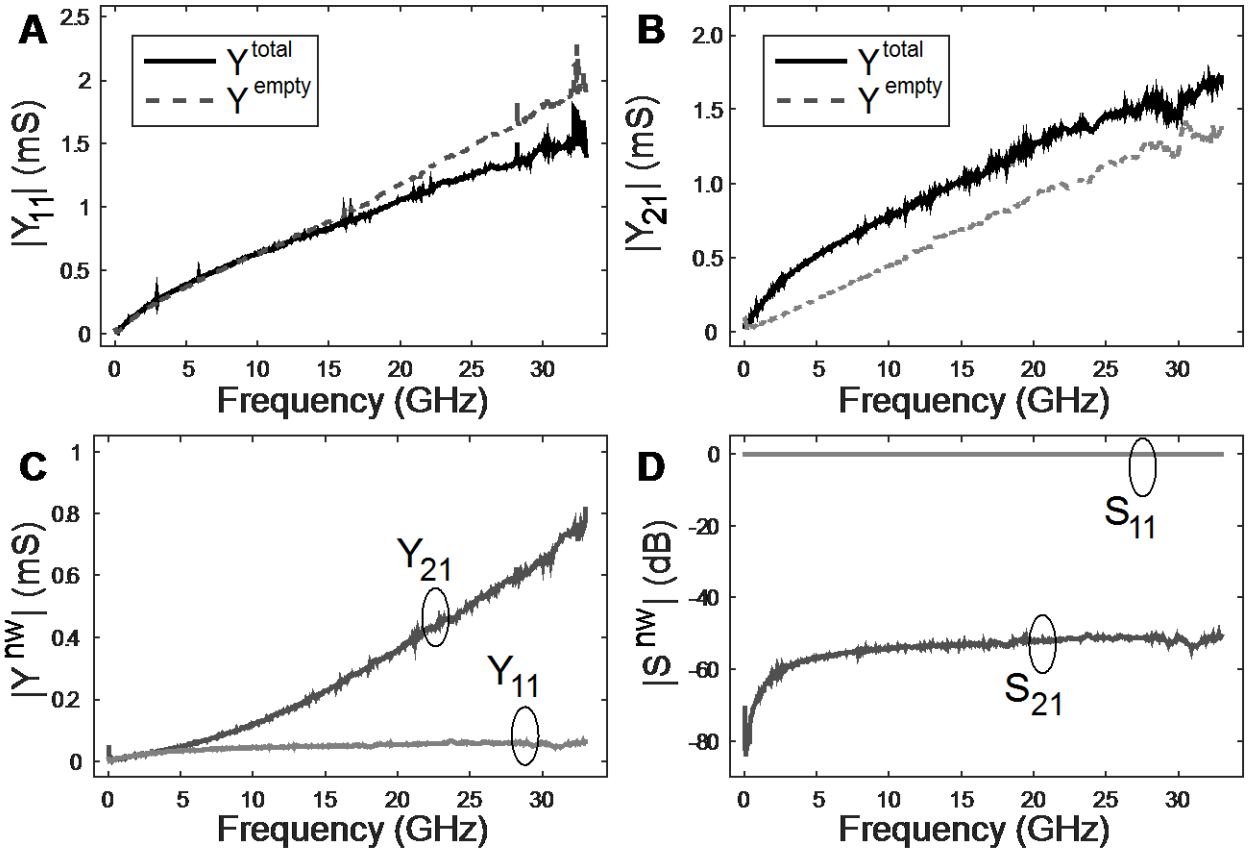
A
B
C
D
Y total
Y empty
|Y11| (mS)
|Y21| (mS)
|Y nw| (mS)
|S nw| (dB)
Y21
Y11
S11
S21
Frequency (GHz)
Frequency (GHz)
Frequency (GHz)
Frequency (GHz)

FIGURE 6-6.

(A) NANOWIRE DEVICE

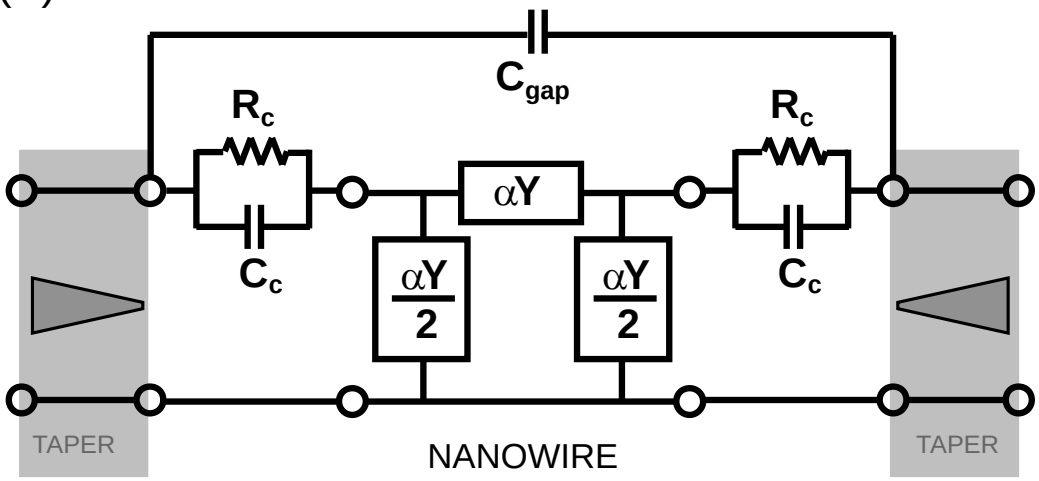

(B) EMPTY DEVICE

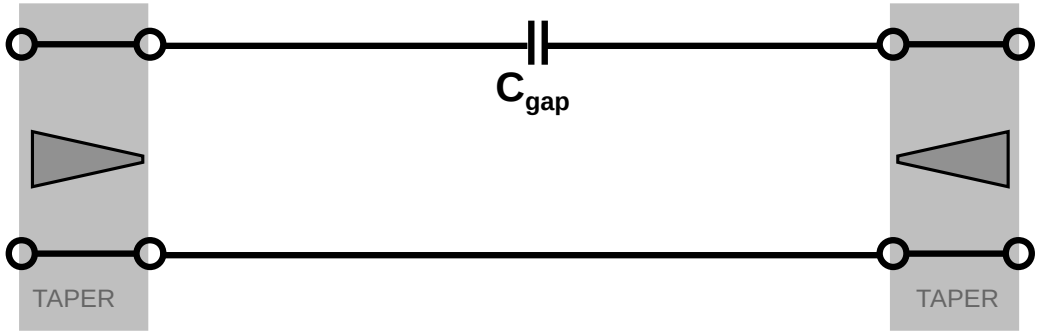

FIGURE 6-7.